Published in final edited form as:
Nat Neurosci. 2008 August ; 11(8): 908–915. doi:10.1038/nn.2157.

Bidirectional temperature-sensing by a single thermosensory neuron in *C. elegans*

Daniel Ramot[1,3], **Bronwyn L MacInnis**[2,4], and **Miriam B Goodman**[1,2]

1*Program in Neuroscience, Stanford University, 279 Campus Dr, Stanford, California 94305, USA*

2*Department of Molecular and Cellular Physiology, Stanford University, 279 Campus Dr, Stanford, California 94305, USA.*

Abstract

Humans and other animals can sense temperature changes as small as 0.1°C. How animals achieve such exquisite sensitivity is poorly understood. By recording from the *C. elegans* thermosensory neurons AFD *in vivo*, we found that cooling closes and warming opens ion channels. We found that AFD thermosensitivity, which exceeds that of most biological processes by many orders of magnitude, is achieved by nonlinear signal amplification. Mutations in genes encoding subunits of a cyclic guanosine monophosphate (cGMP)-gated ion channel (*tax-4* and *tax-2*) and transmembrane guanylate cyclases (*gcy-8*, *gcy-18* and *gcy-23*) eliminated both cooling- and warming-activated thermoreceptor currents, indicating that a cGMP-mediated pathway links variations in temperature to changes in ionic currents. The resemblance of *C. elegans* thermosensation to vertebrate photosensation and the sequence similarity between TAX-4 and TAX-2 and subunits of the rod phototransduction channel raise the possibility that nematode thermosensation and vertebrate vision are linked by conserved evolution.

Sensory abilities have evolved to encourage and support survival in complex natural environments. All animals have the ability to respond to thermal stimuli. As with vision, olfaction, taste and touch sensation, thermosensation relies on the ability of specialized sensory neurons to convert sensory stimuli into changes in ion currents. Given that temperature dependence is a universal feature of ion channel permeation and gating, however, identifying features that set thermosensory neurons apart is a challenge. In principle, these neurons could rely on specialized accessory structures and molecules or on a temperature-dependent enzymatic cascade to enhance thermosensitivity beyond the ordinary temperature dependence that is common to all neurons. Such specialized molecules or structures would act in parallel with the cellular processes that are required for normal neuronal function and whose temperature sensitivity is ordinary.

C. elegans is an excellent animal for probing the cellular machinery responsible for temperature sensation and for identifying both shared and specialized aspects of temperature sensitivity. Many of the neurons required for temperature-guided behaviors are known[1,2] and all of them can be identified in living animals. Our work here concentrates on the AFD neurons, a pair of bilaterally symmetric, bipolar sensory neurons that terminate in modified ciliated endings in

Correspondence should be addressed to M.B.G. (mbgoodman@stanford.edu)..
[3]Present address: D.E. Shaw Research LLC, 120 W. 45th St., 39th Floor, New York, New York 10036, USA.
[4]Present address: Wellcome Trust Sanger Institute, Wellcome Trust Genome Campus, Hinxton, Cambridge, CB10 1SA, UK.

AUTHOR CONTRIBUTIONS

D.R. conducted electrophysiology experiments, analyzed data and wrote the manuscript; B.L.M. prepared mutant strains, conducted behavioral experiments, and contributed to writing; M.B.G. conducted electrophysiology experiments, supervised the project, and wrote the manuscript.

the worm's nose[3,4]. Classical genetic screens[5,6] have identified genes required for temperature sensation and gene expression profiling revealed those expressed in AFD, but not in neighboring chemosensory neurons[7,8].

C. elegans have a complex, temperature-guided behavior that is characterized by experience-dependent plasticity, temperature-dependent migration (thermotaxis) and the ability to accurately track isotherms with 0.1°C precision[9-12]. Thus, *C. elegans* can detect temperature changes of 0.1°C or less. This stimulus, which carries much less energy than a single visible photon, corresponds to a change in thermal energy of $k\Delta T$ or only 10^{-23} J. Such sensitivity appears to be conferred by the AFD thermosensory neurons, as animals that lack AFD[2] or carry mutations that disrupt its development[13,14] have defects in responses to radial thermal gradients. Recently, the response of AFD to thermal stimuli was investigated using genetically encoded Ca^{2+} indicators[12,15-17]. Although these studies showed that intracellular Ca^{2+} rises and falls in synchrony with temporal variations in temperature that are imposed on restrained animals[12,15,16] or produced by animals moving freely on linear thermal gradients[17], the molecular and cellular basis of these responses remain poorly understood. For example, it is not known whether warming opens or closes transduction channels or whether thermal stimuli act directly on them. We paired genetic dissection with *in vivo* whole-cell patch-clamp recording to address these questions. Recording from AFD *in vivo* makes it possible to examine the biophysical and molecular basis of thermotransduction in the presence of accessory proteins and structures that may be needed for temperature sensing.

Five proteins that are localized to the AFD cilium are thought to be elements of a transduction cascade: two cyclic nucleotide–gated (CNG) ion channel proteins (TAX-2 and TAX-4)[18,19], which form a cGMP-gated ion channel in heterologous cells[20], and three transmembrane guanylate cyclases (GCY-8, GCY-18 and GCY-23)[21]. Our data support the hypothesis that cooling and warming are converted into electrical signals in AFD neurons by indirect modulation of the TAX-4/2 cGMP-gated ion channel. As expected from Ca^{2+}-imaging studies and from the accuracy of isothermal tracking, temperature changes as small as 0.1°C elicited both cooling- and warming-activated thermoreceptor currents (ThRCs). We found that ThRCs arose with a response latency of ~100 ms, a finding which favors indirect thermal modulation of the ion channels that carry ThRCs. Our findings indicate that the temperature sensitivity of warming-evoked ThRCs rivaled that of thermoreceptor neurons used by certain snakes to detect warm-blooded prey[22] and exceeded that of transient receptor potential (TRP) channel gating[23,24] by more than ten orders of magnitude.

RESULTS

Wild-type ThRPs and ThRCs

We used a slit-worm preparation[25] and *in vivo* whole-cell patch-clamp recording to measure electrical responses to thermal stimuli in the AFD thermosensory neurons. AFD was visualized in transgenic animals expressing GFP under the control of an AFD-specific promoter. This approach allowed us to unambiguously identify AFD neurons in wild-type and mutant worms and is a major advantage of performing these studies in *C. elegans*. To verify the integrity of AFD neurons and the extent to which saline from the recording pipette penetrated each neuron, we included a diffusible fluorescent dye in the recording pipette (Fig. 1a).

The membrane potential of AFD neurons was depolarized (V_m = −41 ± 2 mV, mean ± s.e.m., n = 5) compared with that of other *C. elegans* neurons[25,26]. Its value was not obviously correlated with holding temperature, indicating that the steady-state temperature is not encoded by membrane potential. To learn more about how AFD detects changes in temperature, we exposed worms to thermal ramps and recorded thermoreceptor potentials (ThRPs). AFD neurons responded to both cooling and warming (Fig. 1b). As described for other *C. elegans*

neurons[25,27], classical action potentials were not observed in AFD neurons. On average, cooling hyperpolarized cells to −70 ± 2 mV (n = 5). Below a threshold temperature, T^*, subsequent warming had no effect on membrane potential. Above T^*, AFD neurons depolarized to –27 ± 1 mV (n = 7). Thus, cooling hyperpolarized AFD neurons by 30 mV and warming above T^* depolarized them by 40 mV.

As suggested by bidirectional ThRPs, thermal ramps produced complex changes in AFD neuron membrane current (Fig. 1c); cooling decreased and warming increased the inward current at −60 mV. Although cooling-evoked ThRCs were small (2.0 ± 0.4 pA, mean ± s.e.m., n = 12), they probably initiate cooling-induced hyperpolarization (Fig. 1b) and may account for cooling-evoked decreases in cytoplasmic Ca^{2+} (refs. 15,17). Warming had no effect on membrane current below T^*. Above T^*, warming elicited a large inward current that reached a peak value at 1 ± 0.2°C (mean ± s.e.m., n = 16) above T^*. Additional cycles of cooling and warming generated a similar sequence of cooling- and warming-evoked ThRCs (Supplementary Fig. 1 online). Thus, AFD provides sufficient information to enable *C. elegans* to detect and distinguish between cooling and warming.

We estimated the response latency for ThRC activation from four rapid temperature steps (0.26 ± 0.06°C) that evoked detectable changes in membrane current (1.8 ± 0.2 pA). In three recordings (two down-steps and one up-step), we measured an average latency of 96 ± 5 ms (n = 3). In the fourth, recorded with K^+-free intracellular saline, the response latency was 132 ms (Fig. 2). This time is sufficient to allow for the generation of a soluble second messenger and favors the idea that temperature indirectly closes and opens ion channels in AFD.

Ordinary versus extraordinary temperature dependence

We hypothesized that AFD neurons share ordinary aspects of temperature dependence with other sensory neurons, but express an extraordinary temperature-sensation pathway responsible for the generation of ThRCs and ThRPs. To explore this idea, we compared the temperature dependence of voltage-activated currents (measured at constant temperature) and temperature-activated currents (measured at constant voltage) in AFD and chemosensory AWA neurons, which are required for chemotaxis toward volatile attractants[28]. Two features make AWA a good choice for this comparison. First, AWA neurons are the only sensory neurons known to provide synaptic input to AFD[4]. Second, similar to AFD neurons, the AWA neurons are bipolar sensory neurons that terminate in ciliated endings[4].

We quantified the effect of temperature on ionic currents by computing the 10-degree temperature coefficient, Q_{10}. For an arbitrary temperature increase, ΔT, this common measure of temperature dependence is given by[29] $Q_{10}=(Q_{\Delta T})^{\frac{10}{\Delta T}}$, where $Q_{\Delta T}$ is the fractional change in rate that is evoked by increasing the temperature by ΔT. The concept of activation energy proposed by Arrhenius provides a more physical description. It states that the reaction rate k depends on activation energy E_a and temperature according to $\ln k = \ln A - E_a/RT$, where A is a temperature-independent constant, T is the absolute temperature and R is the universal gas constant. For a given temperature change, it is simple to calculate Q_{10} from E_a. As the estimate of E_a is derived from data collected at several temperatures, this approach is more resistant to measurement error than methods that rely on measurements taken at two temperatures.

Consistent with the idea that AFD neurons share ordinary aspects of temperature dependence with other neurons, warming increased the amplitude of voltage-activated outward currents in both AFD and AWA. As reported for other *C. elegans* neurons[25], replacing K^+ in the pipette solution with an impermeant cation blocked voltage-gated outward currents (Supplementary Fig. 2 online), suggesting that they are carried by K^+ ions. Such currents activated rapidly and then inactivated along an exponential time course. Both activation and inactivation rates were

higher at warmer temperatures (Fig. 3a). Because activation was too fast to measure accurately, we quantified the temperature dependence of K^+-channel gating from Arrhenius plots of the inactivation rates (Fig. 3b). The Q_{10} for inactivation was 2.8 in AFD and 5.4 in AWA neurons (Fig. 3c), similar to values measured for inactivation of Shaker K^+ channels[30].

Next, we investigated the temperature dependence of membrane current while holding the membrane potential constant at −60 mV. In AFD neurons, but not in AWA neurons, membrane current was altered by cooling and warming (Fig. 4a). We quantified the temperature dependence of membrane current by plotting current versus temperature during warming (Fig. 4b) and transforming these data into Arrhenius plots (Fig. 4c). In AWA neurons, Q_{10} was close to 1, similar to values expected for ion channel permeation and free diffusion of ions in solution[29]. This demonstrates that temperature sensitivity in AFD neurons is probably not conferred by synaptic input from AWA neurons and that temperature has no effect on channel gating at −60 mV in AWA neurons. In AFD neurons, Arrhenius plots consisted of three domains, a steep central domain corresponding to the activation of warming-evoked ThRCs that was flanked by two shallower ones. Apparent Q_{10} values for the central region varied between AFD neuron recordings, but were always greater than 10[21]. This value is reminiscent of that estimated for thermosensory neurons in pit vipers[22]. It is many orders of magnitude larger than the value (20) of thermoreceptor currents measured in mammalian somatosensory neurons in culture[31]. The flanking domains correspond to responses below T^* and to the decrease in current that follows ThRC activation, and were much less temperature sensitive than the central domain, implying that the processes that give rise to ThRC activation are distinct from those that govern recovery.

These findings demonstrate that the temperature dependence of signaling by AFD neurons has an ordinary component that is shared by other neurons (such as AWA) and an extraordinary component that is AFD specific. This steep temperature dependence implies the existence of a nonlinear amplification process that culminates in channel opening. Indeed, the E_a of warming-evoked ThRCs (7,000 ± 500 kJ mol^{-1}, mean ± s.e.m., n = 23) was at least 20-fold greater than the activation energy of thermosensitive ion channels. The cooling-activated ion channel TRPM8, for example, has an E_a equal to 287 kJ mol^{-1} (ref. 24). Although nonlinear amplification has long been recognized as the hallmark of sensory transduction in vision and olfaction, this is the first demonstration that an analogous process operates in temperature sensation.

ThRCs adapt to constant temperature, but not to starvation

As has been seen for warming-evoked Ca^{2+} transients[12], the threshold for warming-evoked ThRCs, T^*, was not fixed, but rather shifted in response to conditioning at constant temperature. Unlike the threshold for Ca^{2+} transients, which adapts on a time scale of hours[12], a few minutes at constant temperature were sufficient to shift T^* under standard recording conditions (Fig. 5a,b). We estimated the time constant of T^* adaptation by fitting the data with a first-order kinetic model, $\frac{\partial T^*}{\partial t} = \frac{1}{\tau}(T - T^*)$, where T is the temperature at time t, and τ is the adaptation time constant. Satisfactory fits (predicted T^* within 0.05°C of measured T^*) were generated by the model with time constants for adaptation to warmer and cooler temperatures of 244 ± 11 s and 518 ± 56 s (mean ± s.e.m., n = 5), respectively. Consistent with rapid adaptation, we found that T^* was tightly correlated with T_{hold}, the temperature at which animals were maintained for ~15 min before application of thermal ramps, but was independent of T_c, the animals' cultivation temperature before the experiment (Fig. 5c). Such rapid adaptation could provide a way to maintain sensitivity to small temperature changes across the full range of physiological temperatures (15–26°C).

One explanation for the difference between the adaptation rates of the threshold for ThRCs and for Ca^{2+} transients is that the process controlling ThRC activation adapts to constant temperature faster than the one responsible for temperature-regulated cytoplasmic Ca^{2+}. Such a difference could reflect a transformation that is mediated by a molecular mechanism in AFD neurons. Alternatively, this difference could arise from limitations in these complimentary cellular recording methods. In particular, we hypothesized that the strength of Ca^{2+} buffering, which probably differs in the two recording methods, could regulate the adaptation rate. We tested this idea by increasing the buffering capacity of our internal solutions, replacing EGTA (10 mM) with BAPTA (20 mM). Under these modified recording conditions, T^* was close to T_c in animals cultivated at 20°C and exposed to holding temperatures between 15 and 21°C ($T^* = 20 \pm 1$°C, $n = 4$). These results imply that the adaptation rate is sensitive to changes in intracellular Ca^{2+} buffering. The true adaptation rate is unknown, as neither whole-cell patch-clamp recording, in which Ca^{2+} buffering is defined by the internal saline, nor Ca^{2+}-imaging techniques, which rely on genetically encoded indicators that could alter Ca^{2+} buffering, represent physiological Ca^{2+}-buffering conditions. Future work is required to determine the true adaptation rate, the nature of the physiological Ca^{2+} buffer and to establish whether behavioral adaptation to temperature shifts, which occurs with a time constant of hours[6,11,12,32], is distinct from or a consequence of sensory adaptation.

Behavioral responses to thermal gradients are abolished by prolonged (>3 h) starvation at a constant temperature[6,9,32]. In contrast, depriving animals of food at constant temperature for >6 h had no apparent effect on ThRCs, voltage-dependent currents or on the relationship between T^* and T_{hold} (Fig. 6). These findings are consistent with the observation that warming-activated Ca^{2+} transients in AFD neurons are retained in starved animals[33] and indicate that information regarding feeding state is stored and exerts its effect on behavior downstream of thermotransduction in AFD neurons.

Cooling closes and warming opens a cGMP-gated ion channel

In mammalian thermosensory neurons, sensory responses to cooling and warming engage distinct TRP channels[34], all of which act to depolarize cells following activation. This scenario probably does not hold for AFD neurons, as cooling and warming had opposite effects on both membrane potential and current (Fig. 1b,c). Cooling drove membrane potential toward E_K (Fig. 1b), which could be achieved by inhibiting an inward current or by activating a K^+ current. Either possibility is compatible with the change in membrane current that was observed at −60 mV. To distinguish between them, we recorded responses to thermal ramps when intracellular K^+ was replaced by *N*-methyl-D-glucamine (NMG^+). Cooling- and warming-evoked ThRCs were retained in K^+-free intracellular saline (Fig. 7a), indicating that cooling inhibits an inward current rather than activating a K^+ current. Calcium influx was not required for cooling- and warming-evoked ThRCs, as such responses persisted in the absence of external Ca^{2+} ions (Fig. 7b and Supplementary Fig. 3 online).

To learn more about the ionic basis of ThRCs, we applied voltage ramps in tandem with thermal ramps. The temperature dependence of K^+ channels in AFD limits this analysis to the hyperpolarized voltages at which these channels are closed (−60 to −30 mV). Over this voltage range, current amplitude decreased with depolarization (Fig. 7c,d) in a fashion that was consistent with a current carried by Na^+ and K^+ ions.

These findings suggest that cooling and warming modulate a common channel, but cannot establish the molecular identity of that channel. So far, TAX-2 and TAX-4 are the only ion channel proteins that are implicated in temperature sensing in *C. elegans*. We found that mutations that eliminated TAX-4 or altered TAX-2 abolished both cooling- and warming-evoked ThRCs in AFD neurons (Fig. 8a and Supplementary Fig. 3) and left voltage-activated currents essentially unchanged (Fig. 8b and Supplementary Fig. 4 online). Thus, we conclude

that TAX-4 and TAX-2 are required for thermotransduction and probably carry ThRCs. The linear *I-V* relationship (Fig. 6d) is consistent with this idea, as recombinant TAX-4/TAX-2 channels also have a nearly linear *I-V* relationship, even in the presence of millimolar divalent ions[19]. Next, we asked whether these proteins were sufficient for temperature sensing by recording from chemosensory AWC neurons, which also co-express TAX-4 and TAX-2 (refs. 18,19). In contrast with AFD neurons, thermal ramps produced no detectable change in membrane current in AWC neurons (Fig. 8a), indicating that the TAX-4/2 channel is not sufficient to confer thermosensitivity at constant voltage.

The extraordinary Q_{10} of warming-evoked ThRCs suggests instead that TAX-4/TAX-2 channels are modulated downstream of a nonlinear amplification pathway, which probably regulates the concentration of intracellular cGMP in a temperature-dependent manner. Consistent with this idea, three transmembrane guanylate cyclase genes, *gcy-8*, *gcy-18* and *gcy-23*, are specifically expressed in AFD neurons[21]. As with the guanylate cyclases that operate in rod photoreceptors[36], these genes act in a redundant manner; triple and double mutants, but not single mutants, have defective behavioral responses to radial thermal gradients[21,35]. Consistent with the idea that guanylate cyclase activity is required for the extraordinary temperature sensitivity of AFD neurons, we found that triple-mutant AFD neurons lacked ThRCs, but retained voltage-activated K^+ currents (Fig. 8 and Supplementary Fig. 4).

As we saw in wild-type animals, depolarization (at constant temperature) activated an outward current in triple mutants that was inactivated following an exponential time course. Between 15.9 and 22.8°C, the rate of outward current inactivation was similar in wild-type and mutant AFD neurons (data not shown). This result suggests that extraordinary and ordinary modes of temperature-dependent signaling in AFD are genetically and molecularly distinct.

DISCUSSION

We combined *in vivo* whole-cell patch-clamp recording with genetic dissection to show that AFD detects temperature changes by means of a molecular pathway that converges on a *tax-4*– and *tax-2*–dependent ion channel. The TAX-4/2 channel is not the only temperature-sensitive channel in AFD: the amplitude and kinetics voltage-gated outward currents are also affected by temperature. Recording from *C. elegans* thermosensory neurons provides a direct way to determine how gene mutations, ion substitution and thermal stimuli affect putative sensory transduction channels, as well as those activated by voltage. One advantage of using whole-cell voltage-clamp recording is its ability to separately examine the temperature-dependence of voltage-activated and thermosensory transduction channels.

Several lines of evidence support the conclusion that temperature indirectly modulates the TAX-4/2 channel via a nonlinear cGMP-dependent signaling cascade. First, the E_a for warming-evoked ThRCs exceeds that of all known ion channels, including mammalian thermosensitive TRP channels[23,24], by at least an order of magnitude. Second, TAX-4 and TAX-2 are necessary, but not sufficient, to confer extraordinary temperature sensitivity, suggesting that TAX-4/2 channels are unlikely to be intrinsically temperature sensitive. In support of this idea, gating by rod photoreceptor CNG channels is independent of temperature[37]. Third, AFD-specific guanylate cyclases are required for ThRCs. Finally, temperature steps open and close channels with a latency of ~100 ms, which is ample time for the local synthesis of a soluble second messenger such as cGMP[20]. On the basis of these findings, we propose that ThRCs arise as a result of nonlinear amplification of a cGMP-dependent signaling cascade and catalyze changes in membrane potential.

Our results demonstrate that AFD is a bidirectional thermosensor that detects tiny changes in temperature, such as those generated by sinusoidal head movements during isothermal tracking. This view is supported by bidirectional changes in cytoplasmic Ca^{2+} (refs. 12,15,17) and indicates that models based on the idea that AFD neurons functions primarily as a heat sensor[2,16,35] cannot fully capture what AFD neurons tell the worms' nervous system about temperature changes.

Many animals, including humans[38,39], have the ability to detect temperature changes on the order of 0.1°C. This ability could arise from a few highly sensitive thermosensory neurons or from summation across a large number of less-sensitive thermosensory neurons. Mammals appear to use the latter strategy, as psychophysical studies demonstrate that sensitivity increases with the skin area stimulated[39] and warming-evoked ThRCs in single thermosensory neurons have Q_{10} values of ~20 (ref. 31). Thus, a temperature increase of 0.1°C will increase inward current by only 3% ($20^{0.1/10}$) in a single mammalian thermosensory neuron. The probability of detection is probably improved by summation. For example, summation across 400 sensory neurons could increase the signal-to-noise ratio 20-fold, yielding the equivalent of a single-cell current that is 60% greater than baseline. This strategy is not available to *C. elegans*, whose entire nervous system is composed of only 302 neurons[4]. Moreover, our data and measurements of AFD Ca^{2+} transients[15,17] indicate that individual AFD neurons can reliably detect temperature changes <0.1°C. Assuming that a single AFD neuron provides a signal that is similar to that of 400 human thermosensory neurons, we estimate that the Q_{10} required for such sensitivity is ~10^{20}, comparable to the Q_{10} measurements reported here. Thus, very high values for Q_{10} are the expected result for any animal that must detect tiny temperature changes with a small number of thermosensory neurons.

Temperature responses in AFD have intriguing similarities to light responses in vertebrate photoreceptors. Both signal the presence of stimuli by modulating the activity of a cGMP-gated channel, use nonlinear amplification to enhance sensitivity, and adapt to maintain sensitivity over a wide range of intensities. Additionally, the TAX-4 α and TAX-2 β CNG channel subunits are orthologues of the α and β subunits of the cGMP-gated channel responsible for phototransduction in vertebrate rods[18,19]. Both cell types elaborate specialized ciliated endings. In rod photoreceptors, the high surface area–to-volume ratio of the outer segment is known to contribute to amplification[40]. It is tempting to speculate that the ~50 villus-like fingers that comprise AFD neuron's ciliated ending serve a similar purpose; they could increase cGMP concentration ~20-fold compared with a spherical structure of the same surface area. In support of this idea, behavioral responses to thermal gradients are disrupted by mutations that alter villus structure[13,14]. A link between light and temperature sensation gains further support from the slime mold *Dictyostelium discoideum*, in which cGMP is a second messenger for both photosensation and thermosensation[41]. Thus, analysis of sensory transduction by AFD sheds light not only on alternative mechanisms of temperature sensation, but also on potentially conserved evolution between photosensation and thermosensation.

METHODS

Nematode strains and culture

To identify AFD, AWA and AWC^{on} neurons in electrophysiology experiments, we used PY1157 *gcy-8*(*oyIs17*), PY1057 *odr-10*(*kyIs37*) and CX3695 *str-2*(*kyIs140*) strains, respectively. Their responses to linear thermal gradients (1°C cm^{-1}) were indistinguishable from wild-type N2 worms (data not shown). Responses to starvation and temperature shifts were similar between N2 and PY1157 (data not shown), indicating that GFP expression in AFD had little, if any, effect on thermal-guided behavior. The *str-2* promoter is expressed in either the left or right AWC neuron[42]. Recordings from AFD in *tax-4*, *tax-2* and triple-mutant *gcy-8gcy-18gcy-23* worms were obtained by crossing *oyIs17* into PR678 *tax-4*(*p678*) III,

PR671 *tax-2*(*p671*) I and IK597 *gcy-8*(*oy44*) *gcy-18*(*nj28*) *gcy-23*(*nj37*) IV to generate mutant worms that express GFP in AFD.

Worms were cultivated with OP-50 *E. coli* following standard procedures[43]. Synchronized populations of young adult worms were used in all experiments. To minimize developmental effects of temperature, all worms were maintained at 20°C until the L4 larval stage. When required, animals were transferred to 15°C, 17°C or to sterile plates at 20°C at least 5 hours before recording.

In vivo electrophysiology

Recordings were carried out as described[25,27], except that the worms were rolled until they lay on their dorsal or ventral sides before immobilization with cyanoacrylate glue (Nexaband, WPI). Warming-evoked ThRC amplitudes were indistinguishable between the left and right AFD neurons ($P = 0.6481$, two-tailed t test).

Recording pipettes were pulled and pressure-polished[44] to achieve resistances of 6–15 MΩ when filled with normal internal saline. Sulforhodamine 101 (10 μM, Molecular Probes) was included in the pipette in all but five early experiments. An EPC-10 amplifier and Patchmaster software (HEKA) were used to acquire data, provide capacitance compensation and correct for liquid junction potentials. During thermal ramps, membrane current and potential were sampled at 1 kHz and filtered at 400 Hz (3-pole Bessel). Responses to voltage steps at constant temperature were digitized at 5 kHz and filtered at 2 kHz. Pulses for calculating whole-cell capacitance and series resistance were digitized at 10 kHz and filtered at 2.9 kHz.

Thermal stimuli

Thermal stimuli were applied by superfusing animals with extracellular saline whose temperature was controlled by a thermoelectric heater/cooler (SC-20/CL-100, Warner Instruments). We measured temperature changes close to the worm's nose using a cylindrical thermistor (TS91-196, McShane) that was only 0.5 mm in diameter and 2.2 mm in length placed <0.5 mm from the worm's nose. Digitized signals from the thermistor provided a record of applied temperature and were also used to periodically adjust settings on the CL-100 controller (via Patchmaster). With this apparatus, we generated temperature ramps between 0.04 and 0.29°C s^{-1}.

Data analysis

We retained recordings that satisfied the following criteria: holding current less than −10 pA (at −60 mV), series resistance <70 MΩ (100 MΩ for recordings with NMG^+ in the pipette) and intact neurites filled with sulforhodamine 101. In standard solutions, series resistance and input capacitance were (mean ± s.d.) 35 ± 9 MΩ and 2.2 ± 0.4 pF ($n = 56$), 25 ± 4 MΩ and 2.8 ± 0.4 pF ($n = 8$) and 29 ± 5 MΩ and 3.1 ± 0.4 pF ($n = 5$) for AFD, AWA and AWC neurons, respectively. Recordings in which internal K^+ was replaced by NMG^+ had an average series resistance of 58 ± 15 MΩ and average input capacitance of 1.7 ± 0.6 pF ($n = 8$). Voltage errors were corrected for liquid junction potentials, but not for uncompensated series resistance. Data analysis used scripts written in Matlab (Mathworks) and Excel (Microsoft).

Voltage-activated currents

Whole-cell capacitance and series resistance were estimated as described[25]. To minimize residual capacity currents, we averaged responses to 12 presentations of a 10-mV pulse, scaled this template to match each applied voltage pulse and subtracted the results from the average ($n = 3$) responses to voltage pulses. Steady-state currents were the average membrane current

in the final 5 ms of the voltage step and peak currents were the maximum detected following the decay of capacity currents that remained after subtraction.

Thermoreceptor potentials and currents

ThRPs, ThRCs and thermistor voltages were smoothed by a 40-ms rectangular window, except for the data that we used to measure ThRC latency, which were smoothed by a 20-ms rectangular window. We determined response polarity and the temperature at which ThRPs and ThRCs achieved their maximum using a MATLAB script to scan the first derivative of the response for the most rapid change in membrane potential (/current) and calculated the amplitude of the change associated with this time point. Brief periods in which the temperature exceeded 25°C were excluded because of an increase in current noise. In all genotypes and cell types, temperature-evoked changes in membrane potential (/current) were classified as a ThRP (/ThRC) if they were larger than 1.1*N*, where *N* is the peak-to-peak noise at constant temperature. The threshold of the response to warming ramps, *T**, was defined as the first 0.05° C temperature interval in which inward potential (/current) noticeably exceeded the baseline membrane potential (/current).

Arrhenius plots were constructed for ThRCs as follows. We normalized ThRC amplitude according to $(I_m - I_o)/I_o$, where I_m is the membrane current and I_o is the membrane current measured after cooling. This procedure was based on the assumption that cooling closes all thermotransduction channels. The activation energy, E_a was calculated from the slope of the Arrhenius plot, which is equal to $-E_a/R$, where R is the gas constant. Q_{10} is then given by $Q_{10} = e^{10Ea/RT1T2}$, where T_1 and T_2 are the temperature boundaries of the fit.

We determined the voltage dependence of warming-evoked ThRCs from voltage ramps (from −80 to +50 mV in 100 ms) applied at 3-s intervals during thermal stimuli. Temperature varied <0.02°C during voltage ramps. To determine average current as a function of voltage and temperature, we measured current at voltages between −60 and −30 mV (in 5-mV increments), computed the average temperature, expressed temperature relative to *T**, normalized current to input capacitance, and calculated the change in current ($\Delta I_m = I_m - I_0$, where I_0 was the average current measured between *T** − 2 and *T** − 0.5°C). Next, we plotted the peak change in current (which occurred near *T** + 1°C) against voltage. Prior to averaging, the change in current was interpolated between *T** ± 2°C at 0.1°C intervals.

Solutions

External saline contained 145 mM NaCl, 5 mM KCl, 5 mM $MgCl_2$, 1 mM $CaCl_2$, 20 mM glucose and 10 mM sodium HEPES, pH adjusted to 7.2 with NaOH. We omitted $CaCl_2$ to produce Ca^{2+}-free external saline. Unless indicated, internal saline contained 125 mM potassium gluconate, 18 mM KCl, 4 mM NaCl, 1 mM $MgCl_2$, 0.6 mM $CaCl_2$, 10 mM potassium HEPES and 10 mM potassium EGTA, pH adjusted to 7.2 with KOH. Osmolarity was ~325 and ~310 mOsm for external and internal saline, respectively. For K^+-free saline, potassium salts were replaced with NMG^+ salts.

Supplementary Material

Refer to Web version on PubMed Central for supplementary material.

ACKNOWLEDGMENTS

We thank C. F. Barrett, T. R. Clandinin, J. Huegenard, A. Y. Katsov, S. Lockery, R. Milo and the Goodman laboratory for comments, G. Wang and Z. Liao for help with genotyping, and P. Sengupta, C. Bargmann, I. Mori and the Caenorhabditis Genetics Center, which is funded by the US National Institutes of Health National Center for Research Resources, for strains. This work was supported by the Baxter, Sloan, McKnight and Klingenstein Foundations

(M.B.G.), the National Science Foundation (M.B.G.), the National Institutes of Health (M.B.G.), a fellowship from the Human Frontiers Science Program (B.L.M.), and a Stanford Graduate Fellowship and Dan David Prize Scholarship (D.R.).

REFERENCES

1. Chung SH, Clark DA, Gabel CV, Mazur E, Samuel AD. The role of the AFD neuron in *C. elegans* thermotaxis analyzed using femtosecond laser ablation. BMC Neurosci 2006;7:30. [PubMed: 16600041]
2. Mori I, Ohshima Y. Neural regulation of thermotaxis in *Caenorhabditis elegans*. Nature 1995;376:344–348. [PubMed: 7630402]
3. Ward S, Thomson N, White JG, Brenner S. Electron microscopical reconstruction of the anterior sensory anatomy of the nematode *Caenorhabditis elegans*. J. Comp. Neurol 1975;160:313–337. [PubMed: 1112927]
4. White JG, Southgate E, Thomson JN, Brenner S. The structure of the nervous system of the nematode *Caenorhabditis elegans*. Philos. Trans. R. Soc. Lond. B Biol. Sci 1986;314:1–340.
5. Mori I. Genetics of chemotaxis and thermotaxis in the nematode *Caenorhabditis elegans*. Annu. Rev. Genet 1999;33:399–422. [PubMed: 10690413]
6. Mohri A, et al. Genetic control of temperature preference in the nematode *Caenorhabditis elegans*. Genetics 2005;169:1437–1450. [PubMed: 15654086]
7. Etchberger JF, et al. The molecular signature and cis-regulatory architecture of a *C. elegans* gustatory neuron. Genes Dev 2007;21:1653–1674. [PubMed: 17606643]
8. Colosimo ME, et al. Identification of thermosensory and olfactory neuron–specific genes via expression profiling of single neuron types. Curr. Biol 2004;14:2245–2251. [PubMed: 15620651]
9. Hedgecock EM, Russell RL. Normal and mutant thermotaxis in the nematode *Caenorhabditis elegans*. Proc. Natl. Acad. Sci. USA 1975;72:4061–4065. [PubMed: 1060088]
10. Ryu WS, Samuel, AD. Thermotaxis in *Caenorhabditis elegans* analyzed by measuring responses to defined thermal stimuli. J. Neurosci 2002;22:5727–5733. [PubMed: 12097525]
11. Luo L, Clark DA, Biron D, Mahadevan L, Samuel AD. Sensorimotor control during isothermal tracking in *Caenorhabditis elegans*. J. Exp. Biol 2006;209:4652–4662. [PubMed: 17114399]
12. Biron D, et al. A diacylglycerol kinase modulates long-term thermotactic behavioral plasticity in *C. elegans*. Nat. Neurosci 2006;9:1499–1505. [PubMed: 17086178]
13. Perkins LA, Hedgecock EM, Thomson JN, Culotti JG. Mutant sensory cilia in the nematode *Caenorhabditis elegans*. Dev. Biol 1986;117:456–487. [PubMed: 2428682]
14. Cassata G, et al. The LIM homeobox gene *ceh-14* confers thermosensory function to the AFD neurons in *Caenorhabditis elegans*. Neuron 2000;25:587–597. [PubMed: 10774727]
15. Clark DA, Biron D, Sengupta P, Samuel AD. The AFD sensory neurons encode multiple functions underlying thermotactic behavior in *Caenorhabditis elegans*. J. Neurosci 2006;26:7444–7451. [PubMed: 16837592]
16. Kimura KD, Miyawaki A, Matsumoto K, Mori I. The *C. elegans* thermosensory neuron AFD responds to warming. Curr. Biol 2004;14:1291–1295. [PubMed: 15268861]
17. Clark DA, Gabel CV, Gabel H, Samuel AD. Temporal activity patterns in thermosensory neurons of freely moving *Caenorhabditis elegans* encode spatial thermal gradients. J. Neurosci 2007;27:6083–6090. [PubMed: 17553981]
18. Coburn CM, Bargmann CI. A putative cyclic nucleotide–gated channel is required for sensory development and function in *C. elegans*. Neuron 1996;17:695–706. [PubMed: 8893026]
19. Komatsu H, Mori I, Rhee JS, Akaike N, Ohshima Y. Mutations in a cyclic nucleotide–gated channel lead to abnormal thermosensation and chemosensation in *C. elegans*. Neuron 1996;17:707–718. [PubMed: 8893027]
20. Komatsu H, et al. Functional reconstitution of a heteromeric cyclic nucleotide–gated channel of *Caenorhabditis elegans* in cultured cells. Brain Res 1999;821:160–168. [PubMed: 10064800]
21. Inada H, et al. Identification of guanylyl cyclases that function in thermosensory neurons of *Caenorhabditis elegans*. Genetics 2006;172:2239–2252. [PubMed: 16415369]

22. Bullock TH, Diecke FP. Properties of an infrared receptor. J. Physiol. (Lond.) 1956;134:47–87. [PubMed: 13377311]
23. Liu B, Hui K, Qin F. Thermodynamics of heat activation of single capsaicin ion channels VR1. Biophys. J 2003;85:2988–3006. [PubMed: 14581201]
24. Brauchi S, Orio P, Latorre R. Clues to understanding cold sensation: thermodynamics and electrophysiological analysis of the cold receptor TRPM8. Proc. Natl. Acad. Sci. USA 2004;101:15494–15499. [PubMed: 15492228]
25. Goodman MB, Hall DH, Avery L, Lockery SR. Active currents regulate sensitivity and dynamic range in *C. elegans* neurons. Neuron 1998;20:763–772. [PubMed: 9581767]
26. O'Hagan, R. Components of a mechanotransduction complex in C. elegans touch receptor neurons: an in vivo electrophysiology study. Columbia University; 2005. PhD Dissertation
27. O'Hagan R, Chalfie M, Goodman MB. The MEC-4 DEG/ENaC channel of *Caenorhabditis elegans* touch receptor neurons transduces mechanical signals. Nat. Neurosci 2005;8:43–50. [PubMed: 15580270]
28. Bargmann CI, Hartwieg E, Horvitz HR. Odorant-selective genes and neurons mediate olfaction in *C. elegans*. Cell 1993;74:515–527. [PubMed: 8348618]
29. Hille, B. Ion Channels of Excitable Membranes. 3rd ed.. Sinauer Associates; Sunderland, Massachusetts: 2001.
30. Nobile M, Olcese R, Toro L, Stefani E. Fast inactivation of Shaker K^+ channels is highly temperature dependent. Exp. Brain Res 1997;114:138–142. [PubMed: 9125459]
31. Vyklicky L, et al. Temperature coefficient of membrane currents induced by noxious heat in sensory neurones in the rat. J. Physiol. (Lond.) 1999;517:181–192. [PubMed: 10226158]
32. Chi CA, et al. Temperature and food mediate long-term thermotactic behavioral plasticity by association-independent mechanisms in *C. elegans*. J. Exp. Biol 2007;210:4043–4052. [PubMed: 17981872]
33. Kodama E, et al. Insulin-like signaling and the neural circuit for integrative behavior in *C. elegans*. Genes Dev 2006;20:2955–2960. [PubMed: 17079685]
34. Dhaka A, Viswanath V, Patapoutian A. TRP ion channels and temperature sensation. Annu. Rev. Neurosci 2006;29:135–161. [PubMed: 16776582]
35. Kuhara A, et al. Temperature sensing by an olfactory neuron in a circuit controlling behavior of *C. elegans*. Science 2008;320:803–807. [PubMed: 18403676]
36. Baehr W, et al. The function of guanylate cyclase 1 and guanylate cyclase 2 in rod and cone photoreceptors. J. Biol. Chem 2007;282:8837–8847. [PubMed: 17255100]
37. Bucossi G, Nizzari M, Torre V. Single-channel properties of ionic channels gated by cyclic nucleotides. Biophys. J 1997;72:1165–1181. [PubMed: 9138564]
38. Hardy JD, Oppel TW. Studies in temperature sensation. III. The sensitivity of the body to heat and the spatial summation of the end organ responses. J. Clin. Invest 1937;16:533–540. [PubMed: 16694500]
39. Kenshalo DR, Decker T, Hamilton A. Spatial summation on the forehead, forearm and back produced by radiant and conducted heat. J. Comp. Physiol. Psychol 1967;63:510–515. [PubMed: 6064398]
40. Pugh EN Jr, Lamb TD. Amplification and kinetics of the activation steps in phototransduction. Biochim. Biophys. Acta 1993;1141:111–149. [PubMed: 8382952]
41. Darcy PK, Wilczynska Z, Fisher PR. The role of cGMP in photosensory and thermosensory transduction in *Dictyostelium discoideum*. Microbiology 1994;140:1619–1632. [PubMed: 8075804]
42. Troemel ER, Sagasti A, Bargmann CI. Lateral signaling mediated by axon contact and calcium entry regulates asymmetric odorant receptor expression in *C. elegans*. Cell 1999;99:387–398. [PubMed: 10571181]
43. Brenner S. The genetics of *Caenorhabditis elegans*. Genetics 1974;77:71–94. [PubMed: 4366476]
44. Goodman MB, Lockery SR. Pressure polishing: a method for reshaping patch pipettes during fire polishing. J. Neurosci. Methods 2000;100:13–15. [PubMed: 11040361]

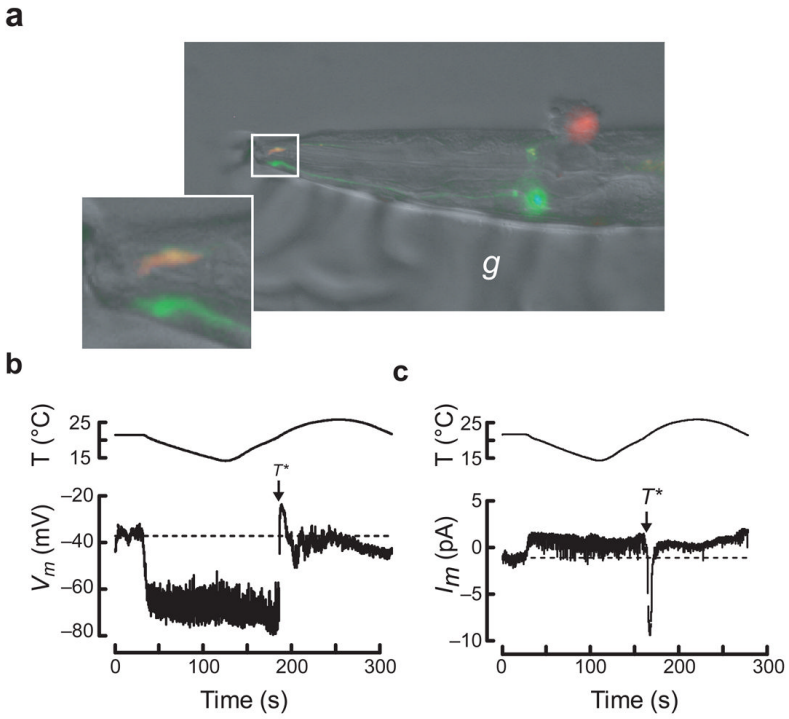

Figure 1.

in vivo recording from wild-type *C. elegans* thermosensory neurons. (**a**) Micrograph of a dissected AFD neuron following whole-cell patch-clamp recording. The top (red), but not the bottom (green), AFD neuron was labeled by sulforhodamine 101 delivered by the recording pipette. The inset shows the worm's nose and labeled sensory endings of both AFD neurons. The micrograph is a dual-color fluorescence image digitally overlaid on a differential interference constrast (DIC) image of the same preparation. Anterior is to the left. *g*, glue used to immobilize the worm. (**b**) AFD receptor potential in response to a thermal ramp. (**c**) AFD receptor current in response to a thermal ramp (V_h = −60 mV). Data acquisition was interrupted periodically to reprogram the temperature controller (indicated by gaps in the traces).

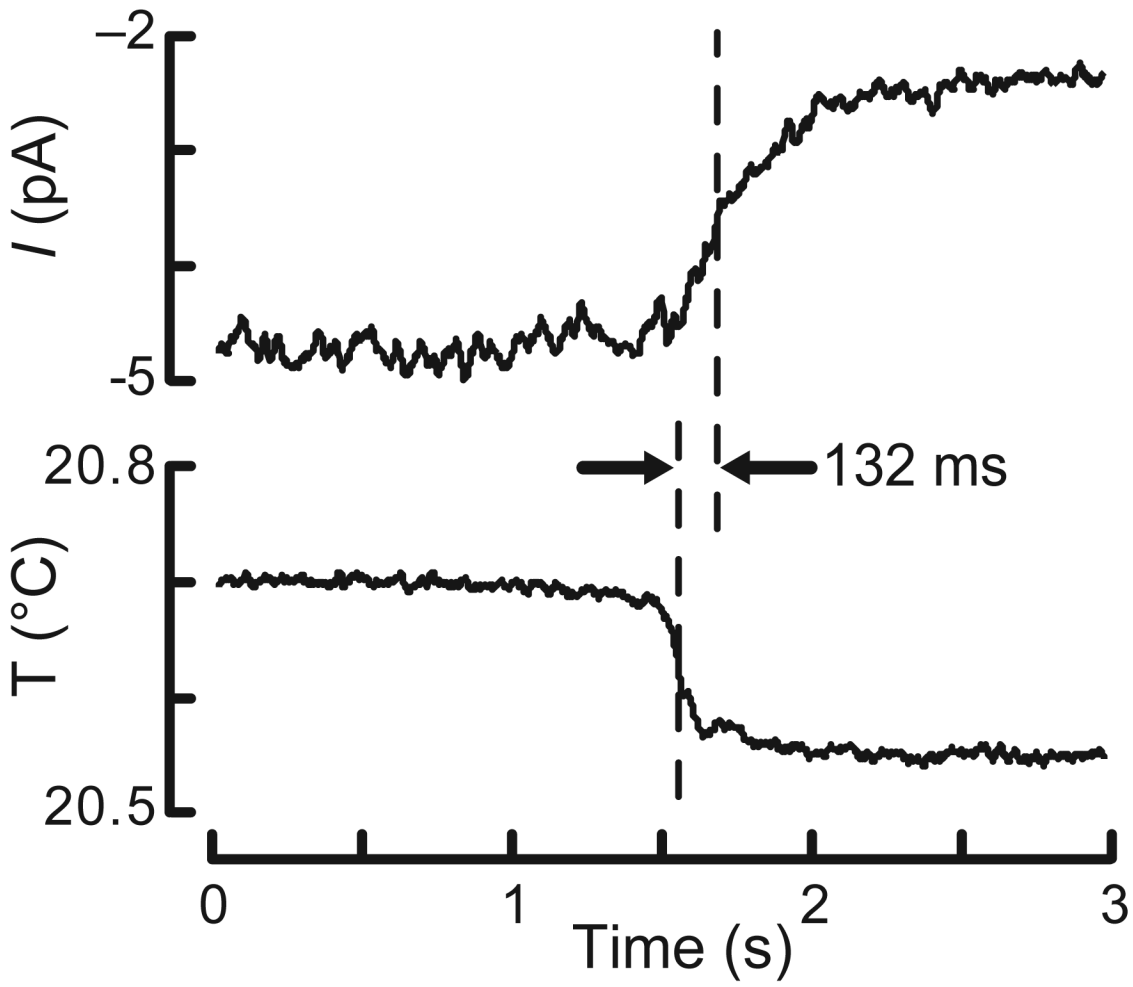

Figure 2.
ThRC response latency. The decrease in inward current (top) evoked by a rapid cooling step (bottom) is shown. The latency was the time difference between the half maximum points of both traces. Similar results were obtained in a total of four AFD recordings.

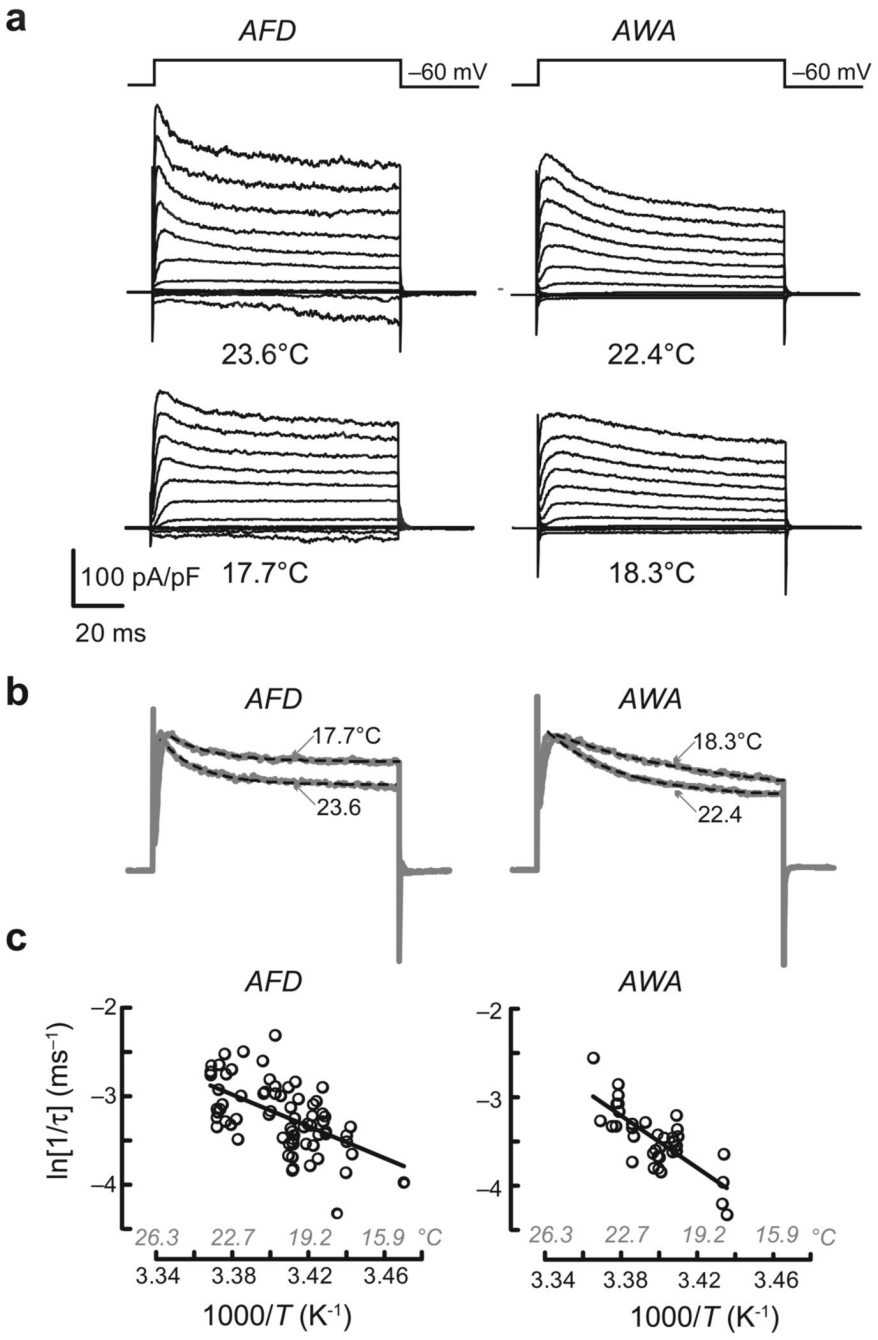

Figure 3.

Temperature dependence of voltage-gated currents in thermosensory (AFD) and chemosensory (AWA) neurons. (**a**) Voltage-activated currents in AFD and AWA neurons elicited by voltage pulses between −110 and +110 mV (in 20-mV increments) from V_h = −60 mV at two temperatures. (**b**) Normalized current evoked by a voltage pulse to +50 mV at two temperatures in AFD (left) and AWA (right) neurons. Data replotted from **a**. Dashed lines are exponential fits to the data (AFD: τ = 15.6 and 17.7 ms at 23.6°C and 17.7°C, respectively; AWA: τ = 29.9 and 64.8 ms at 22.4°C and at 18.3°C, respectively). (**c**) Arrhenius plots of inactivation rates for currents evoked by voltage steps to +30 mV in AFD (left) and AWA (right) neurons. Data were pooled from 22 AFD and 9 AWA recordings. E_a was 74 and 122 kJ mol^{-1} for AFD and

AWA, respectively. Q_{10} was measured for the full range of temperatures tested and was 2.8 in AFD and 5.4 in AWA.

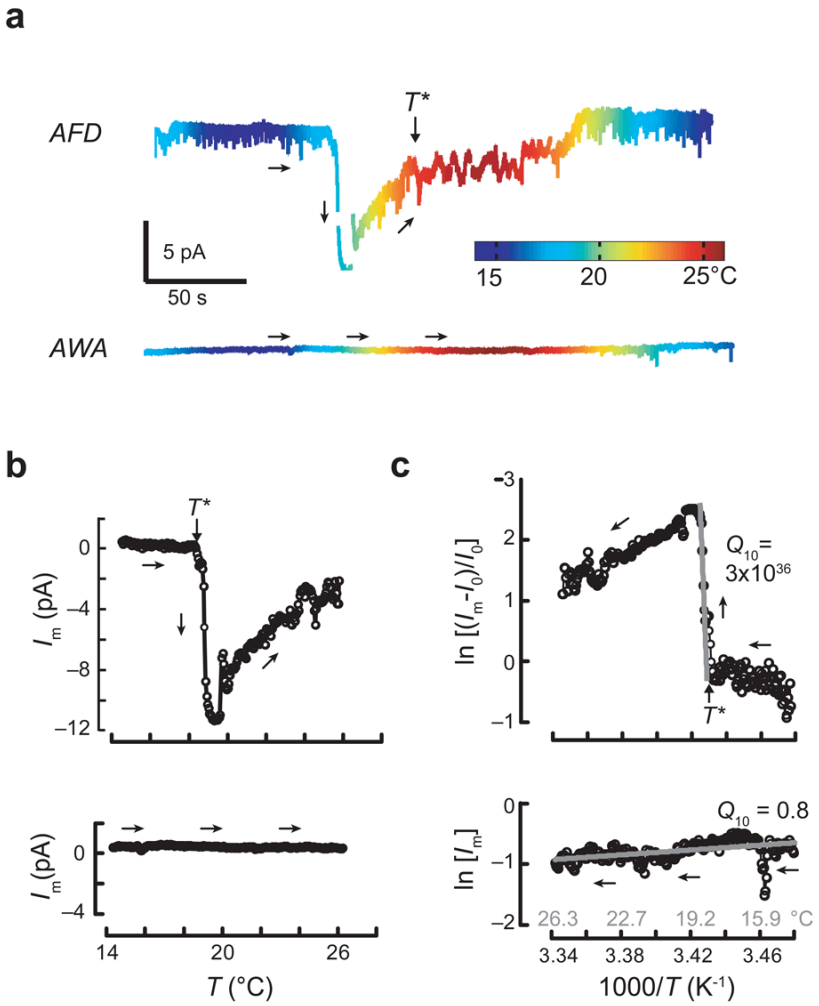

Figure 4.

Thermoreceptor currents in AFD and AWA neurons at −60 mV. (**a**) Change in membrane current evoked by thermal ramps applied to AFD (top) and AWA (bottom) neurons plotted versus time (trace color encodes temperature). (**b**) Membrane current in AFD (top) and AWA (bottom) neurons plotted as a function of temperature during warming. Circles are the average current in each 0.05°C interval. (**c**) Arrhenius plots of warming-evoked currents in AFD (top) and AWA (bottom) neurons. Arrows indicate the time trajectory. V_{hold} = −60 mV. E_a was 5,900 and −16 kJ mol^{-1} for AFD and AWA neurons, respectively. Similar results were obtained in a total of 23 AFD and 8 AWA recordings.

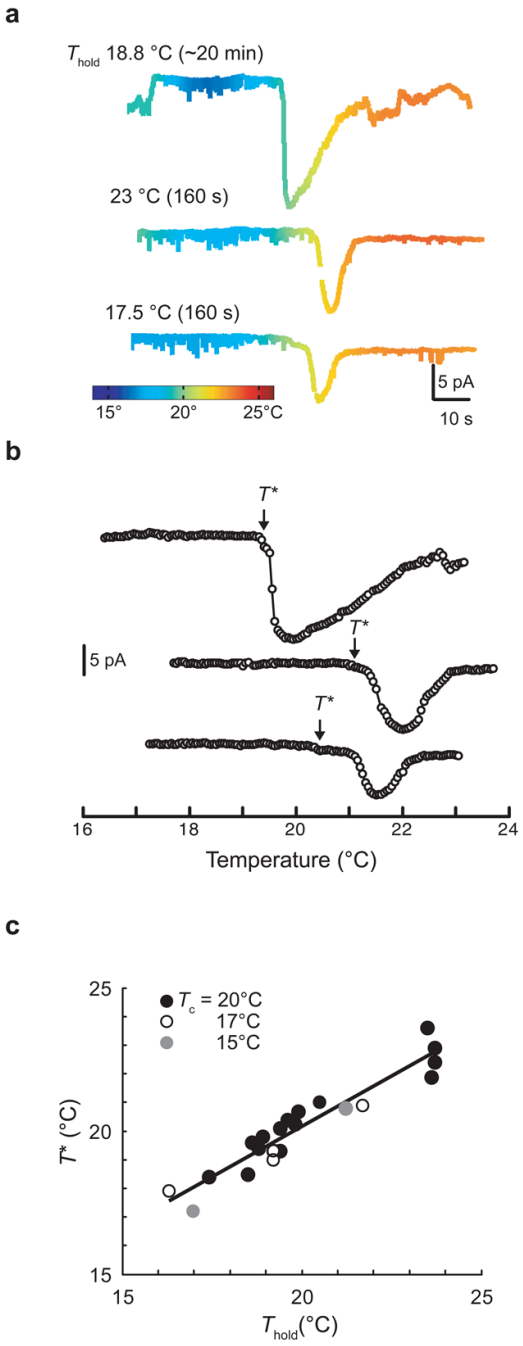

Figure 5.

ThRC adaptation. (**a**) ThRCs elicited by three consecutive thermal ramps applied to a single AFD neuron. Between stimulus ramps, T_{hold} was held at the value indicated for the duration given in parentheses. (**b**) Warming-evoked ThRCs plotted against temperature (same recording as in **a**). Open circles are average current in 0.05°C intervals. (**c**) T^* plotted against T_{hold} for AFD recordings obtained from animals cultivated at 15 (n = 2), 17 (n = 4) and 20°C (n = 15). Points represent T^* measured from the first stimulus ramp applied in each individual recording. The line is a least-squares fit to the data (R^2 = 0.91).

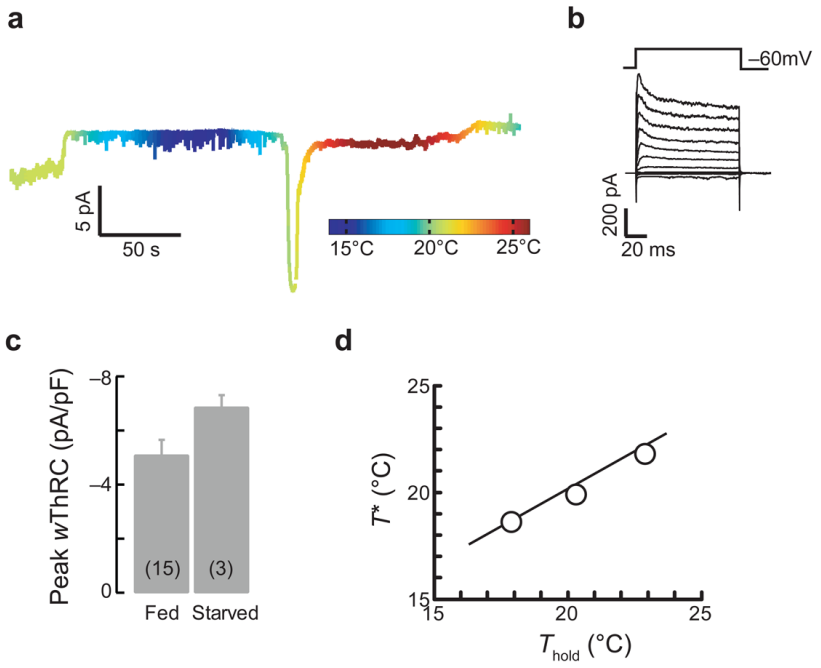

Figure 6.

AFD signals are similar in well-fed and starved animals. (**a**) Membrane current at V_h = −60 mV evoked by a thermal ramp in an animal starved at 20°C for 6.25 h. (**b**) Voltage-gated activated currents in the same cell as in **a**. (**c**) Peak warming-evoked ThRC amplitudes in well-fed and starved animals grown at 20°C. Bars are mean ± s.e.m. and were not significantly different (P = 0.193, t test). The number of recordings is indicated in parentheses. (**d**) T^* plotted against T_{hold} for AFD recordings obtained in starved animals. The smooth line is the fit from Figure 5c.

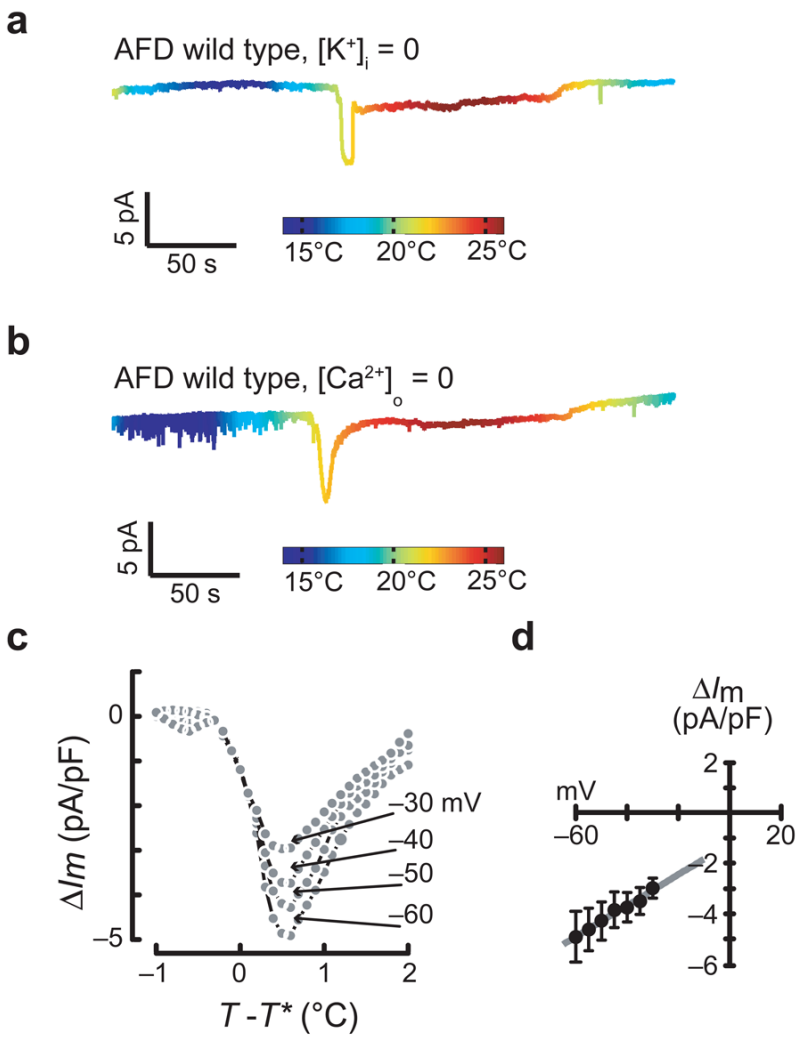

Figure 7.

Ionic properties of AFD thermoreceptor currents (ThRCs). (**a**,**b**) Membrane current at V_h = −60 mV evoked by a temperature ramp in the absence of internal K^+ (**a**) and external Ca^{2+} (**b**). (**c**) Average warming-evoked current at four membrane potentials plotted versus relative temperature. Each point represents the average current (n = 3) measured at that voltage during the voltage ramp plotted against the average temperature during the voltage ramp. (**c**) Peak ThRC *I-V* relationship derived from the data in **c**. Error bars are s.e.m; smooth line is a linear fit to the data (R^2 = 0.98).

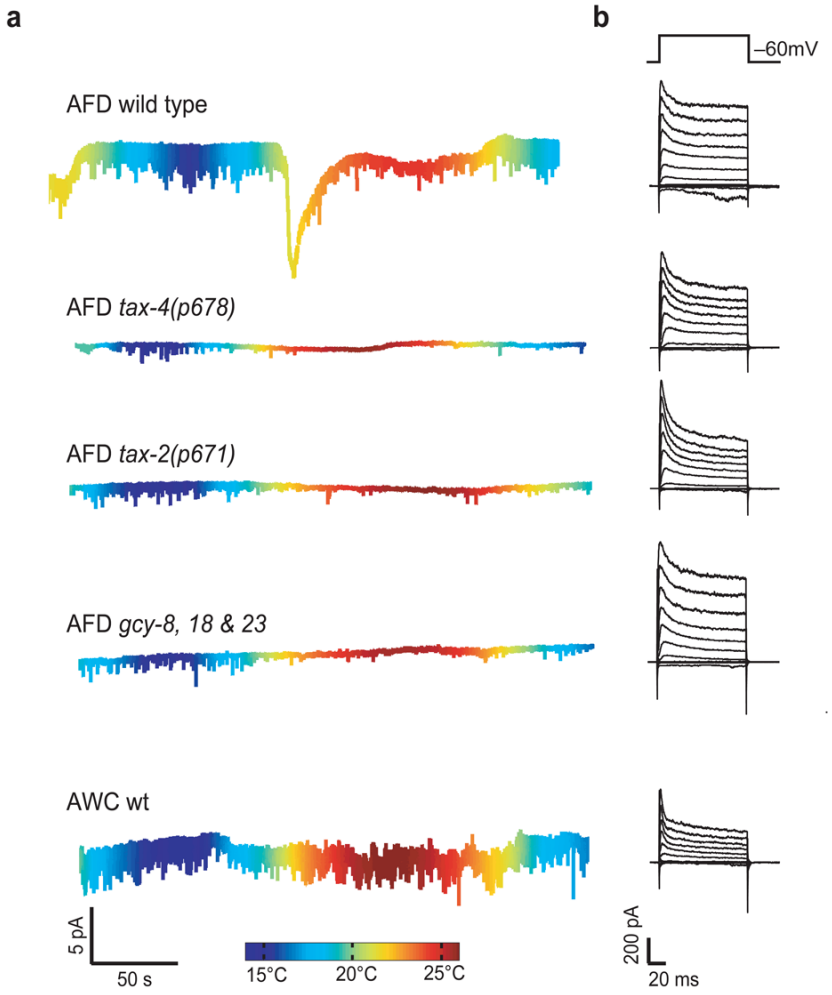

Figure 8.

Thermoreceptor currents (ThRCs) are observed in wild-type, but not in *tax-4*, *tax-2* or triple mutant *gcy-8;gcy-18;gcy-23* AFD neurons, nor in AWC neurons. (**a**) Membrane current at −60 mV in response to thermal ramps. Cell type and genotype are indicated for each trace (and apply across traces in **b**). Color encodes temperature. (**b**) Membrane currents elicited by voltage pulses between −110 and +110 mV (in 20-mV increments) from V_h = −60 mV for the cells shown in **a**. T_c = 20°C for all recordings except wild-type AFD neurons, where T_c = 15°C.